Theoretical analysis of Young-type electron interference in $He^{2+} + H_2$ collisions using a semiclassical model

G. Oliviéro, V. Pestel, L. Bottey, M. Philippe, and F. Frémont
Université de Caen, CIMAP, 6, Boulevard du Maréchal Juin, 14050 Caen Cedex, France
(Received 16 September 2014; published 21 October 2014)

A four-body semiclassical model is developed to describe interferences observed in the angular distribution of Auger electrons emitted after double capture in 30-keV $He^{2+} + H_2$ collisions. The present model is based on both the corpuscular and wave behaviors of the emitted electron. The corpuscular aspect is used to determine the trajectories of the collision partners, while the wave behavior occurs only in the determination of the phase shift. The results of the calculation are found to reproduce the experiment remarkably well. Series of maxima and minima are found in the angular distribution, with periods that are close to the experimental values. In addition, at a fixed angle, oscillations in the energy distribution are clearly evidenced in both the experiment and calculation.

DOI: 10.1103/PhysRevA.90.042711 PACS number(s): 34.70.+e, 34.50.−s, 32.80.Hd, 34.10.+x

I. INTRODUCTION

Since the famous hypothesis by Louis de Broglie [1] that a wave can be associated with a massive moving particle, many experiments have been conducted to show the wave-particle duality [2–6]. In particular, since 2001, Young-type interferences caused by electrons scattering on atomic or molecular targets have been experimentally [7–10] and theoretically [11–13] studied.

Very recently, a theoretical description of an original experiment has been proposed [14]. The process

$$\begin{aligned} He^{2+} + H_2(1\sigma) &\rightarrow He^{**}(2lnl',n \geqslant 2) + H^+ + H^+ \\ &\rightarrow He^+(1s) + H^+ + H^+ + e^- \end{aligned} \quad (1)$$

has been analyzed. A He^{2+} projectile first captures both H_2 molecular target electrons on $2lnl'$ doubly excited states. After the capture, one electron is ejected mainly by Auger effect, with energies in the range 30–40 eV. Two groups of peaks centered at energies of ∼33 and 35 eV, associated with $2s^2\,{}^1S$ and $(2p^2\,{}^1D{-}2s2p\,{}^1P)$ terms, respectively, can be separated, while peaks located at energies larger than 36 eV and associated with $2lnl'$ $(n \geqslant 3)$ configurations are also observed.

The electron emitted at angles close to 180° with respect to the incident beam direction (also called backward angles) scatters on both recoiling protons that play the role of the two holes in a Young double slit experiment with photons. Interferences are thus produced, and well-defined oscillations were predicted. The realization of the present proposal was realized a few years later, and oscillations with a period of ∼17° could be observed in the angular distribution of emitted electrons [15–17], in agreement with the theoretical prediction [14] based on quantum mechanics. To get more information on the oscillations themselves, a polynomial function was used to fit the main angular dependency [17] and subtracted. The result, also shown in Fig. 3 of Ref. [17], is presented in Fig. 1 (empty circles).

To interpret the results, an analysis based on quantum mechanics was performed. Briefly, the autoionization amplitude is separated into reduced amplitude which takes into account the decay of the autoionizing state, namely $2s^2\,{}^1S$, and a factor $\mathcal{A}$ which describes the influence of the protons onto the emitted electrons. Following Barrachina and Zitnik [14],

$$\begin{aligned} \mathcal{A} \approx -i \int_0^\infty &\{1 + [D(\overrightarrow{r_N}) - 1]\cos(\overrightarrow{s} \cdot \overrightarrow{r_H})\} \\ &\times t^{2i/k_T} e^{-(1-i\varepsilon)\Gamma t/2} dt. \end{aligned} \quad (2)$$

In this expression, $D(\overrightarrow{r_N})$ is a distortion factor which depends on the distance r_N between the projectile and the ionized target center of mass, and the reduced energy ε is defined as $\varepsilon = 2/\Gamma\,(E - E_o)$, where $1/\Gamma$ and E_o are the lifetime and the resonant energy of the $2s^2\,{}^1S$ state. The quantities $\overrightarrow{s}$ and $\overrightarrow{r_H}$ refer to the momentum transfer and the vector characterizing the distance between one proton and the H_2^{2+} center of mass, respectively. The vector $\overrightarrow{s}$ is defined by $\overrightarrow{s} = \overrightarrow{k} - k\overrightarrow{r_N}/r_N$, where $\overrightarrow{k}$ is the electron momentum. The calculation was performed assuming an average distance $r_H \sim 8$ a.u., defined at time $t = 2/\Gamma \sim 400$ a.u. [14]. In the frame of this approximation, the interference pattern could be evidenced (Fig. 1 of Ref. [14]). Moreover, simple formulas could be used to fit the experimental data (small dashed lines in Fig. 1). Briefly, the oscillation term is governed by the well-known Debye-Ehrenfest term $\sin\delta/\delta$ [18,19], with $\delta = 2V_e^L d_{HH}\cos(\theta/2)$. In this expression, V_e^L is electron velocity in the laboratory frame, and d_{HH} is the average distance between the two protons. It has been recently shown that the best fit occurs when the three configurations are taken into account [20].

When relation (2) is fully applied, and after subtraction of the intensity by a polynomial function, no oscillations are observed (full line of Fig. 1) [21]. This surprising result can be understood as follows. Whatever the expression of the distortion factor $D(\overrightarrow{r})$, the interference term is governed by $\cos(\overrightarrow{s} \cdot \overrightarrow{r_H})$, which depends on time via the vectors $\overrightarrow{r_H}$ and $\overrightarrow{r_N}$. The addition of infinite cosine terms destroys the interference pattern. The result is quite similar to the one we would obtain using white light in photon interference experiments.

To get more detailed information on the pseudoperiods of the oscillation pattern, fast Fourier transform (FFT) has been applied on the angular distribution. Figure 2 shows the results of the FFT on the experiment (open circles), the fitting result (dashed curve), and the quantum calculation (full curve). Surprisingly, even if one Bessel function could be enough to fit

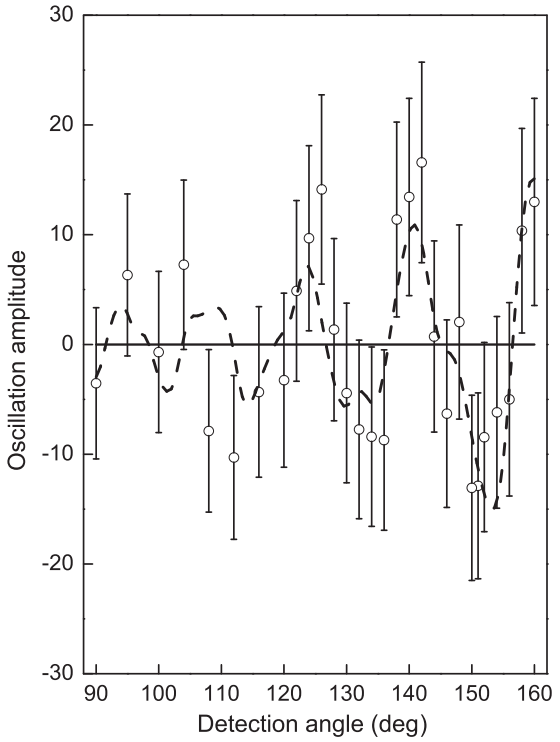

FIG. 1. Oscillation term in the angular distribution of Auger electrons following 30-keV $He^{2+} + H_2$ collision. Open circles: experiment. Dashed curve: fit of the experimental oscillations. Full curve: result of the calculation using relation (2).

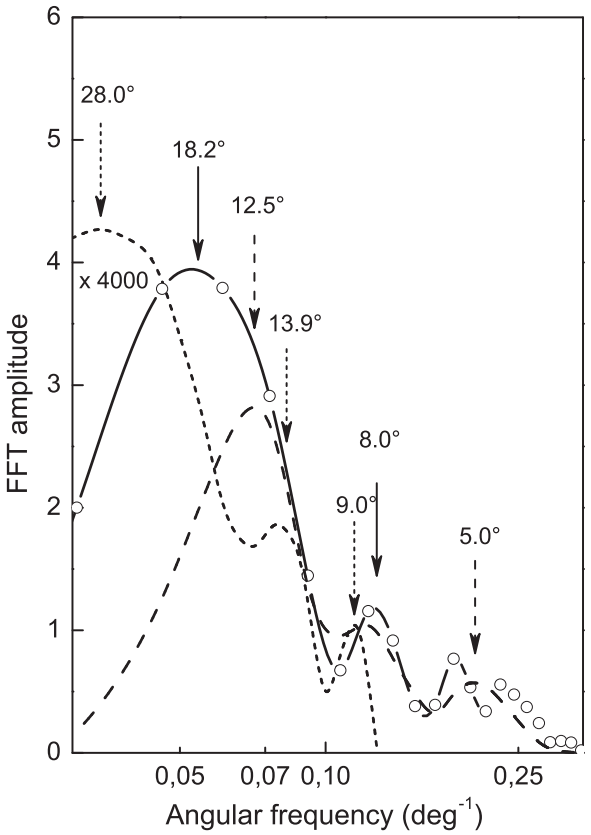

FIG. 2. Fast Fourier transform (FFT) of the angular distributions shown in Fig. 1. Open circles: experiment. Dashed curve: fit of the experiment. Full line: full calculation using relation (2). The latter result is multiplied by 4000 to emphasize the structures. The maxima are depicted by arrows.

the angular distribution [15] in the first approximation, three maxima, located at 0.055, 0.125, and 0.2 $\deg^{-1}$, are clearly evidenced. This shows that interferences are due to the combination of the three configurations. The fitting curve (dashed curve) presents also three maxima. Whereas the maxima associated with the $2p^2\,{}^1D$ and $2s2p\,{}^1P$ terms are close to the experimental one, the maximum associated with the $2s^2\,{}^1S$ term is located at 0.08 $\deg^{-1}$, which disagrees with the experimental value of 0.055 $\deg^{-1}$. Maxima are also present in the FFT of the quantum calculations. However, the amplitude is multiplied by a factor of 4000, and the positions of the maxima are far from the experimental one.

Since no other quantum theory is available to describe the interference phenomenon in such slow collisions, a four-body semiclassical model (4BSCM) has been developed, based on the corpuscular and wave aspects of the emitted electrons. The idea originates from macroscopic-scale experiments developed a few years ago [22]. In this experiment, a droplet of silicon oil falls on a vertically vibrated bath of the same fluid. Under specific conditions, the droplet "walks" on the surface, generating waves. Thus, the so-called walker is constituted of a corpuscle and a wave. The authors let individual droplets walk and cross a slit. Despite the chaotic behavior of the trajectories, the number of droplets was shown to follow a law that clearly shows the wave character of the droplet. Indeed, a diffraction figure was obtained, similar to what we would observe with light.

The corpuscular-wave association gave us the idea to build a model resembling the experiment described above. The model we constructed is first based on the corpuscular aspect and then on the wave behavior of the electrons, meaning that each aspect is independently treated.

In Sec. II, the model is described in detail. Approximations will be discussed. Then, in Secs. III and IV, angular distributions and energy distributions derived from the present model will be shown and compared with the experimental results.

II. SEMICLASSICAL MODEL

A. Initial conditions

Suppose there is an electron, located at $\vec{r_e^m} = \vec{v_p} t_e^m + \vec{b}$ from the H_2^{2+} center of mass, which is emitted with a velocity $\vec{v_e^m}$ in the projectile frame (Fig. 3). Assuming, to simplify, an impact parameter $b = 0$, it follows that $\vec{r_e^m} = z_e^m \vec{u_z}$.

It was verified that the influence of b on the angular distribution is weak. Indeed, the introduction of a nonzero impact parameter only induces a shift in the angular distribution and does not change its shape.

At time $t_e^m = 0$, where the electron is emitted, the quantity v_e^m is chosen so that, before scattering on the protons, Gaussian curves with natural widths Γ_S, Γ_P, and Γ_D [23,24] are used to describe the three configurations $2s^2\,{}^1S$, $2s2p\,{}^1P$, and $2p^2\,{}^1D$, respectively. Since no information is known concerning the relative weight of the initial populations of the configurations,

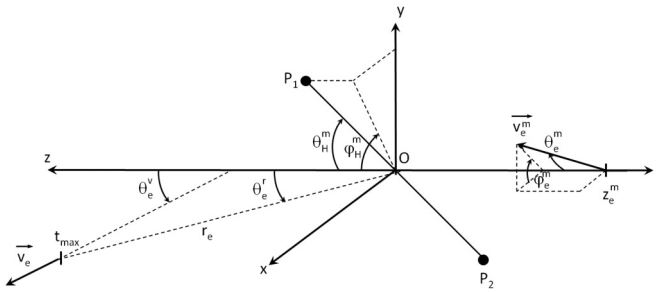

FIG. 3. Schematic three-dimensional view of initial and final conditions of an emitted electron in the field of two protons P_1 and P_2. At $t = 0$, the angles θ_e^m and φ_e^m characterize the direction of the velocity $\overrightarrow{v_e^m}$ of the electron, which is located at z_e^m from O. The angles $\theta_{\rm H}^m$ and $\varphi_{\rm H}^m$ characterize the position of the doubly ionized target. At $t = t_{\rm max}$, the electron is at a distance $r_{\rm e}$ from O and has a velocity $\overrightarrow{v_e}$. The quantities θ_e^V and θ_e^r are the angles between the incident beam direction and the final electron velocity $\overrightarrow{v_e}$ and position $\overrightarrow{r_e}$, respectively.

they are assumed to be equally distributed. The angles θ_e^m and φ_e^m which characterize the direction of $\overrightarrow{v_e^m}$, as well as the angles $\theta_{\rm H}^m$ and $\varphi_{\rm H}^m$ which characterize the position of the doubly ionized target, are randomly chosen in order to obtain spherical distributions. More precisely, the cosine of θ_e^m and $\theta_{\rm H}^m$ are chosen in the range [–1;1] in order to get homogeneous distributions. The distance r_e^m is also randomly chosen, weighting by a decreasing exponential function $e^{-\Gamma_i t}$ ($i = S, P, D$), which takes into account the Auger deexcitation probability. Since the interference phenomenon is assumed to begin when the electron is emitted, the initial distance $d_{\rm HH}^m$ between the two hydrogen ions is calculated at time t_e^m. Finally, the remaining projectile electron is considered to be frozen.

B. Calculation of the trajectories

From these initial conditions, Hamilton equations for the motion of He^+, the two protons, and the emitted electron are numerically solved using the Runge-Kutta method of order 4, with an adaptive step [25]. This method has been shown to be very efficient in many cases (see, for example, Ref. [26]). The Hamiltonian writes (atomic units are used)

$$H = \sum_{i=1}^{2} \frac{p_i^2}{2M} + \frac{p_e^2}{2} + \frac{p_{\rm He}^2}{2M_{\rm He}} + \sum_{i=1}^{2} \left(-\frac{1}{\|\overrightarrow{r_i} - \overrightarrow{r_e}\|} + \frac{2}{\|\overrightarrow{r_i} - \overrightarrow{r_{\rm He}}\|} \right) + \frac{1}{\|\overrightarrow{r_1} - \overrightarrow{r_2}\|}. \quad (3)$$

In the above expression, $\overrightarrow{p_i}$, $\overrightarrow{p_e}$, and $\overrightarrow{p_{\rm He}}$ are the momenta of the protons, the electron, and the projectile; M and $M_{\rm He}$ are the proton and projectile masses; and $\overrightarrow{r_i}$, $\overrightarrow{r_e}$, and $\overrightarrow{r_{\rm He}}$ characterize the positions of the protons, the electron, and the projectile. Finally, the time evolution of the system is

$$\frac{dp_{i\alpha}}{dt} = -\frac{\partial H}{dr_{i\alpha}}; \quad \frac{dr_{i\alpha}}{dt} = \frac{\partial H}{dp_{i\alpha}}. \quad (4)$$

where i refers to the four moving particles, and α indicates the three components of the vectors along the three coordinate axes.

It is supposed that each particle acts with the three other particles, except He^+ which interacts only with the protons and not with the ejected electron, since the Auger electron velocity at $t = 0$ is the one it has at infinity. To obtain good statistics, the number of calculated trajectories was fixed to 500 000. Integration time was chosen as follows: Let us call θ_e^V and θ_e^r the angles between the incident beam direction and the final electron velocity $\overrightarrow{v_e}$ and position $\overrightarrow{r_e}$, respectively; calculation was ended when the condition $\theta_e^V - \theta_e^r < 0.1^\circ$ was fulfilled. This condition corresponds to an integration time $t_{\rm max}$ of the order of 1000 a.u.

C. Determination of the phase shift

At the end of the integration time, suppose two electrons are located at M_1 and M_2, characterized by their respective angles (θ_1,φ_1) and (θ_2,φ_2). After rotation of M_1 and M_2 by φ_1 and φ_2, respectively, around the (Oz) axis, the problem to solve is confined to the $(y0z)$ plane (Fig. 4). The points obtained after rotation are called M_{1y} and M_{2y}. Their respective coordinates are $(y_1/\sin\varphi_1, z_1)$ and $(y_2/\sin\varphi_2, z_2)$, as shown in Fig. 4. Similarly to notations in Fig. 3, θ_i^V and θ_i^r are the angles between the incident beam direction and the final electron velocity $\overrightarrow{v_i}$ and position $\overrightarrow{r_i}$.

The electron that is detected on M_{1y} reaches the detector before the electron which reaches M_{2y}. The latter is therefore delayed compared to the first electron, and the missing distance for the electron to reach the detector is $\delta_{12} = M_{2y}M'_{2y}$, which is easily calculated as a function of the coordinates and the final angles.

Since double capture is not taken into account in the calculation, the probability that an electron is emitted by Auger effect is equal to unity. Thus, the amplitude associated with an electron i is

$$A_i = e^{-iE_i(t_{\rm max} - \frac{\delta_{1i}}{V_i})}, \quad (5)$$

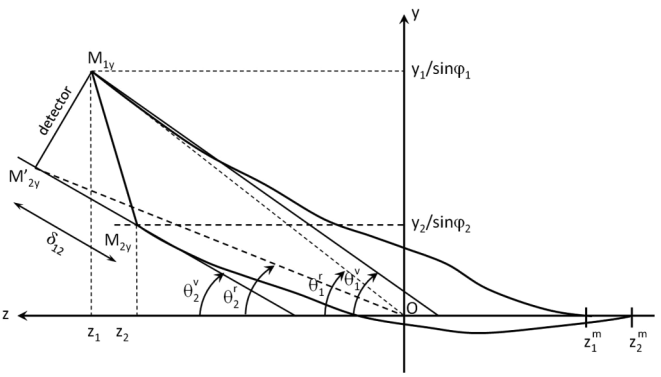

FIG. 4. Schematic two-dimensional view of two electron trajectories. An electron is detected at M_{1y} on the detector, while the second electron is delayed. The missing distance is $\delta_{12} = M_{2y}M'_y$. The projection of the trajectories on a plan is used to increase the statistics.

where E_i and V_i are the final electron energy and velocity, respectively, and δ_{1i}/v_i is the phase shift induced by the delay. The total amplitude $A(\theta_d)$ at a fixed angle $\theta_d \pm \Delta\theta_d$, where $\Delta\theta_d = 2^\circ$ is the experimental angular resolution, is the sum of the individual amplitudes A_i. Finally, the intensity is determined using $I(\theta_d) = |A(\theta_d)|^2$.

III. ANGULAR DISTRIBUTION OF AUGER ELECTRONS

Figure 5(a) shows the Auger electron angular distribution calculated using the model described above, in the range 90°–180°. At angles larger than 170°, the intensity is found to be maximum. In the range 90°–170°, series of maxima and minima are clearly observed. The shape of the present intensity strongly differs from the experimental one (see, for example, Fig. 2 of Ref. [17]), since no pseudosinusoidal oscillation is clearly evidenced. However, a refined analysis using the FFT method shows [filled squares in Fig. 5(b)] three structures whose maxima, depicted by arrows, are located at frequencies corresponding to pseudoperiods of about 15.2°, 10.0°, and 7.4°. Comparison with frequencies deduced from experimental (open circles in Fig. 5) shows a qualitative agreement. Despite the observed differences between the structure maxima, the calculated pseudoperiods are consistent with experimental pseudoperiods (18.2°, 8.0°, and 5.0°). Consequently, the present result supports the idea that the series of maxima and minima seen in the calculated angular distribution are caused by Young-type interferences.

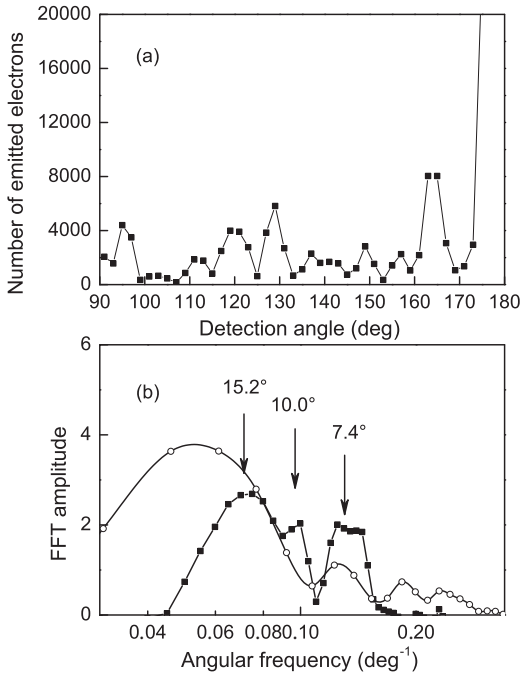

FIG. 5. Auger electron angular distribution (a) calculated using the 4BSC model (see text), in the range 90°–180°. Series of maxima and minima are clearly observed. (b) presents the FFT of the calculation (full squares). The experimental FFT is also shown for comparison. Three maxima are observed, giving evidence for Young-type interferences in the calculated angular distribution.

IV. ENERGY DISTRIBUTION AT A FIXED ANGLE

Since the present model is able to reproduce at least qualitatively the angular distribution of Auger electrons, the question arises whether it can provide information on the Auger spectra at fixed angles. Since the energy resolution is the best at large angles [15], the spectra were calculated at a detection angle of 160°. Figure 6(a) presents the result of the calculation, convoluted by an apparatus function, for the $2s^2\,{}^1S$ configuration and the $(2s2p\,{}^1P - 2p^2\,{}^1D)$ configurations, located at 12.4 and 13.5 eV, respectively. The dashed curve is the result of the calculation when the interferences between the three configurations are not taken into account, while the full curve is the calculation result when interferences between the three terms are introduced. In the latter case, oscillations in the energy distribution are clearly seen, especially between 10.5 and 13 eV, with an average period of ~0.5 eV.

The same FFT procedure was applied to the present results. Figure 6(b) shows the FFT calculation result for both angular distributions represented in Fig. 6(a). Without any interferences, the FFT amplitude decreases from 1 to 5 eV^{-1}. The visible oscillations are mainly due to the shape of the structures and to the fact that the energy range is not infinite. When interferences are included, the shape of the amplitude

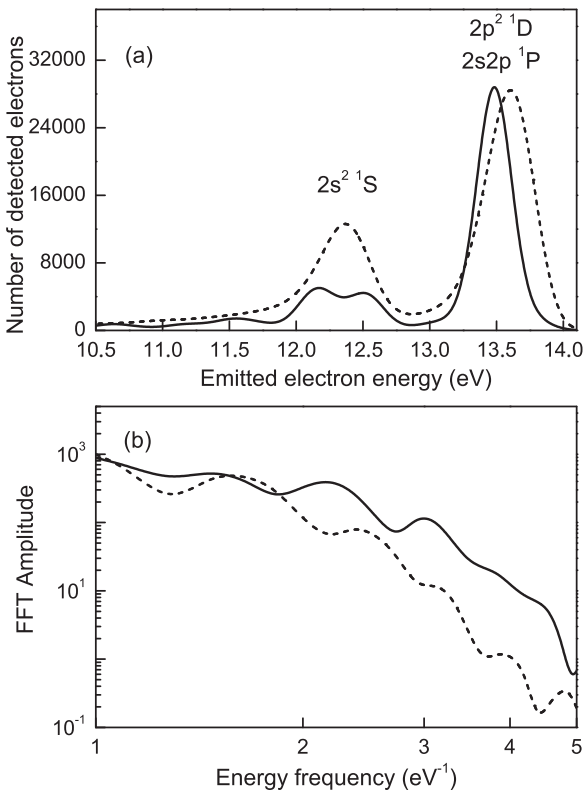

FIG. 6. Energy distribution of Auger electrons following deexcitation of $2lnl'$ configurations, calculated using the 4BSC model (a), for a detection angle of 160°. Dashed curve: no interferences between the structures. Full curve: interferences between Auger peaks are taken into account. (b) shows the respective FFT amplitudes. When interferences between Auger peaks are taken into account, a large structure is observed, with an average frequency of the order of 4 eV^{-1}.

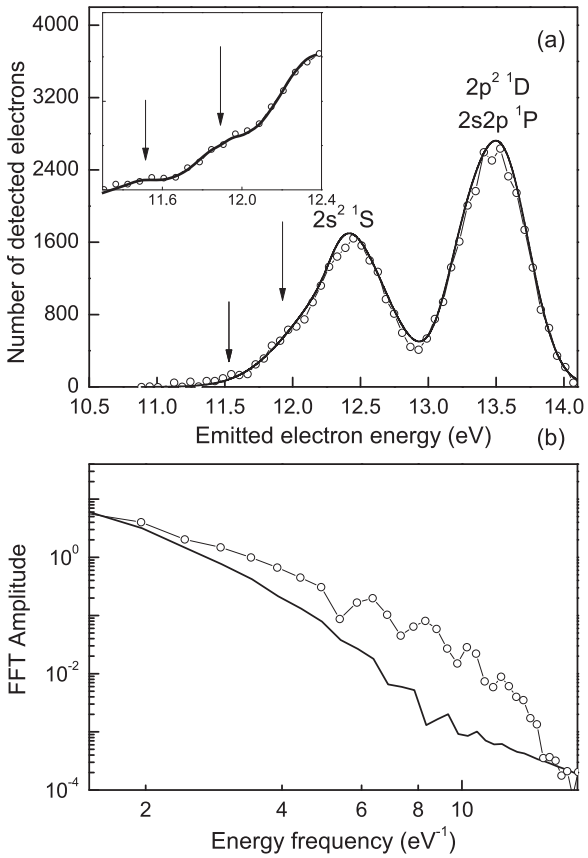

FIG. 7. Experimental energy distribution of Auger electrons following deexcitation of $2lnl'$ configurations [open circles in (a)], at a detection angle of 160°. The full curve fits the experimental structures. (b) shows the respective FFT amplitudes. Full curve: FFT amplitude for the fit. Open circles: FFT amplitude associated with the experiment. The inset in (a) increases the visibility of the oscillating structures. The full line in the inset is used as a guide for the eye.

differs from the previous one. It is seen that the amplitude is larger between 2 and 5 eV^{-1} than that found without any interferences. The average frequency is of the order of 4 eV^{-1}, giving rise to a pseudoperiod of 0.25 eV.

If the present model is valid, such oscillations would be also present in the experiment. In Fig. 7(a), a typical spectrum obtained at 160° is presented (open circles). A careful inspection of the spectra [the inset of Fig. 7(a)] reveals additional structures at energies of about 11.5 and 11.8 eV, with small amplitude compared to that found in the calculation.

Since the presence of oscillations is not obvious, the FFT method was again used to get evidence for possible structures. First, to compare with experiment, the experimental spectra are fitted using distorted Gaussian curves [20]. The result of the FFT amplitude is given in Fig. 7(b) for the experimental energy distribution (open circles) and the fitting curves (solid lines). Whereas the latter amplitude decreases monotonously when frequency increases, a large structure appears between 2 and 20 eV^{-1}, showing that oscillations are present. The agreement with calculation is reasonable, except that the range of frequencies is shifted. Indeed, the average frequencies for the experiment and the calculation are 3.93 and 2.28 eV^{-1}, respectively, corresponding to average pseudoperiods of 0.25 and 0.44 eV. Such structures in the energy spectra were clearly observed several decades ago in collision between He^+ ions and He target, at a projectile energy of 1400 eV [27]. Oscillating structures with a period of about 1 eV could become visible because the spectra were measured at 180° with respect to the incident beam direction so that the Doppler effect was minimized. The authors showed that the oscillatory structure can be described by an approximate semiclassical formulation of a postcollision interaction model, in which the possible interference of contributions from different coherently excited autoionization states in the ejected-electron spectrum was taken into account. Consequently, our model which also takes into account interferences between autoionizing states is consistent with previous analysis.

V. CONCLUSION

In the present paper, a 4B-SC model has been developed and applied to collisions between Auger electrons and two protons, in order to describe interference phenomena observed experimentally in the angular distribution of Auger electrons following double electron capture in 30-keV $He^{2+} + H_2$ collisions. In contrast with calculation based on quantum mechanics, the present model is able to reproduce, at least qualitatively, but also quantitatively, the angular distribution of Auger electrons, as well as energy distribution of Auger electrons at a fixed angle. At present, there is no explanation for this surprising result. A more detailed analysis of electron trajectories that lead to maximum and minimum intensity is thus needed.

Since only autoionization has been studied, the next step in our future work will be to include the double electron capture process in the calculation. Indeed, if the separation of the primary process (double capture) and the postcollision process (autoionization) is well adapted to calculate, for example, total or partial cross sections, both processes have to be included to study interferences, since interference phenomena are already present before the collision in the H_2 molecule itself. The classical treatment of the whole collision is thus a challenge, which first requires that we correctly simulate the H_2 molecule, by the inclusion of electron-electron interaction.

[1] L. de Broglie, C. R. Acad. Sci. **177**, 507 (1923).
[2] H. Rauch, W. Treimer, and U. Bonse, Phys. Lett. A **47**, 369 (1974).
[3] O. Carnal and J. Mlynek, Phys. Rev. Lett. **66**, 2689 (1991).
[4] M. Arndt, O. Nairz, J. Vos-Andreae, C. Keller, G. van der Zouw, and A. Zeilinger, Nature **401**, 680 (1999).
[5] S. Gerlich, S. Eibenberger, M. Tomandl, S. Nimmrichter, K. Hornberger, P. J. Fagan, J. Tüxen, M. Mayor, and M. Arndt, Nat. Commun. **2**, 263 (2011).

[6] M. R. Andrews, C. G. Townsend, H.-J. Miesner, D. S. Durfee, D. M. Kurn, and W. Ketterle, Science **275**, 637 (1997).
[7] N. Stolterfoht, B. Sulik, V. Hoffmann, B. Skogvall, J. Y. Chesnel, J. Rangama, F. Frémont, D. Hennecart, A. Cassimi, X. Husson, A. L. Landers, J. A. Tanis, M. E. Galassi, and R. D. Rivarola, Phys. Rev. Lett. **87**, 023201 (2001).
[8] D. Misra, U. Kadhane, Y. P. Singh, L. C. Tribedi, P. D. Fainstein, and P. Richard, Phys. Rev. Lett. **92**, 153201 (2004).
[9] S. Hossain, A. L. Landers, N. Stolterfoht, and J. A. Tanis, Phys. Rev. A **72**, 010701(R) (2005).
[10] O. Kamalou, J.-Y. Chesnel, D. Martina, F. Frémont, J. Hanssen, C. R. Stia, O. A. Fojón, and R. D. Rivarola, Phys. Rev. A **71**, 010702(R) (2005).
[11] L. Nagy, L. Kocbach, K. Pora, and J. Hansen, J. Phys. B **35**, L453 (2002).
[12] L. Sarkadi, J. Phys. B **36**, 2153 (2003).
[13] M. Galassi, R. D. Rivarola, and P. D Fainstein, Phys. Rev. A **70**, 032721 (2004).
[14] R. O. Barrachina and M. Žitnik, J. Phys. B **37**, 3847 (2004).
[15] J.-Y. Chesnel, A. Hajaji, R. O. Barrachina, and F. Frémont, Phys. Rev. Lett. **98**, 100403 (2007).
[16] F. Frémont, A. Hajaji, R. O. Barrachina, and J.-Y. Chesnel, J. Phys.: Conf. Ser. **88**, 012020 (2007).
[17] F. Frémont, S. Suarez, R. O. Barrachina, A. Hajaji, N. Sisourat, A. Dubois, and J. Y. Chesnel, Nucl. Instrum. Methods Phys. Res. B **267**, 206 (2009).
[18] P. Debye, Ann. Phys. (Leipzig, Ger.) **351**, 809 (1915).
[19] P. Ehrenfest, Amsterdam Acad. **23**, 1132 (1915).
[20] F. Frémont, *Young-Type Interferences with Electrons. Basics and Theoretical Challenges in Molecular Collision Systems*, Springer Series on Atomic, Optical, and Plasma Physics Vol. 77 (Springer, Berlin, 2013).
[21] B. Sorgunlu Frankland, Ph.D. thesis, Université de Caen, 2013.
[22] Y. Couder and E. Fort, Phys. Rev. Lett. **97**, 154101 (2006).
[23] A. Bordenave-Montesquieu, A. Gleizes, and P. Benoit-Cattin, Phys. Rev. A **25**, 245 (1982).
[24] J. P. Giese, M. Schultz, J. K. Swenson, H. Schöne, M. Benhenni, S. L. Varghese, C. R. Vane, P. F. Dittner, S. M. Shafroth, and S. Datz, Phys. Rev. A **42**, 1231 (1990).
[25] R. Abrines and I. Percival, Proc. Phys. Soc. **88**, 861 (1966).
[26] D. J. W. Hardie and R. E. Olson, J. Phys. B: At. Mol. Phys. **16**, 1983 (1983).
[27] R. Morgenstern, A. Niehaus, and U. Thielmann, J. Phys. B: At. Mol. Phys. **10**, 1039 (1977).